Regulation of the epithelial Na^+ channel by paraoxonase-2

Received for publication, March 8, 2017, and in revised form, July 14, 2017 Published, Papers in Press, August 2, 2017, DOI 10.1074/jbc.M117.785253

Shujie Shi[‡], Teresa M. Buck[§], Carol L. Kinlough[‡], Allison L. Marciszyn[‡], Rebecca P. Hughey[‡¶‖], Martin Chalfie[**], Jeffrey L. Brodsky[§], and Thomas R. Kleyman[‡¶‡‡1]

From the [‡]Renal-Electrolyte Division, Department of Medicine, [§]Department of Biological Sciences, [¶]Department of Cell Biology, [‖]Department of Microbiology and Molecular Genetics, and [‡‡]Department of Pharmacology and Chemical Biology, University of Pittsburgh, Pittsburgh, Pennsylvania 15261 and the [**]Department of Biological Sciences, Columbia University, New York, New York 10027

Edited by Henrik G. Dohlman

Paraoxonase-2 (PON-2) is a membrane-bound lactonase with unique anti-oxidative and anti-atherosclerotic properties. PON-2 shares key structural elements with MEC-6, an endoplasmic reticulum–resident molecular chaperone in *Caenorhabditis elegans*. MEC-6 modulates the expression of a mechanotransductive ion channel comprising MEC-4 and MEC-10 in touch-receptor neurons. Because *pon-2* mRNA resides in multiple rat nephron segments, including the aldosterone-sensitive distal nephron where the epithelial Na^+ channel (ENaC) is expressed, we hypothesized that PON-2 would similarly regulate ENaC expression. We observed PON-2 expression in aquaporin 2–positive principal cells of the distal nephron of adult human kidney. PON-2 also co-immunoprecipitated with ENaC when co-expressed in HEK293 cells. When PON-2 was co-expressed with ENaC in *Xenopus* oocytes, ENaC activity was reduced, reflecting a reduction in ENaC surface expression. MEC-6 also reduced ENaC activity when co-expressed in *Xenopus* oocytes. The PON-2 inhibitory effect was ENaC-specific, as PON-2 had no effect on functional expression of the renal outer medullary potassium channel. PON-2 did not alter the response of ENaC to extracellular Na^+, mechanical shear stress, or α-chymotrypsin–mediated proteolysis, suggesting that PON-2 did not alter the regulation of ENaC by these factors. Together, our data suggest that PON-2 regulates ENaC activity by modulating its intracellular trafficking and surface expression.

The mammalian paraoxonase (PON)[2] family consists of three highly conserved genes (*pon-1*, *pon-2*, and *pon-3*) that encode enzymes with hydrolase and lactonase activities (1). PON-1 and PON-3 are secreted proteins that are expressed primarily in liver (1, 2). In contrast, PON-2 is a membrane-bound protein that is ubiquitously expressed in many tissue types and organs, including heart, lung, and kidney (3, 4). Among different cell types, PON-2 expression has been found within mitochondria, the perinuclear region, the endoplasmic reticulum (ER), and the plasma membrane (5–7). PON-2 appears to have a protective role against oxidative stress-induced apoptosis and lipid peroxidation (6–8). PON-2–deficient mice showed increased mitochondrial oxidative stress and inflammatory markers, in association with enhanced diet-induced atherogenesis (5, 9). A gene-silencing study suggested a role for PON-2 in reducing blood pressure by a dopamine receptor-dependent inhibition of NADPH oxidase activity, preventing excessive reactive oxygen species production within renal proximal tubules (10). Nonetheless, despite growing interest in the PON family, the physiologic functions of PON-2 remain largely unidentified.

PON-2 shares structural features with MEC-6 (mechanosensory abnormality-6), a type-II transmembrane protein found in the nematode *Caenorhabditis elegans* (11, 12). MEC-6 is required for the worm's gentle touch response, an avoidance behavior mediated by an ion channel complex expressed in *C. elegans* touch-receptor neurons (13, 14). At the core of this mechanotransductive complex are MEC-4 and MEC-10, two members of the epithelial Na^+ channel (ENaC)/degenerin family of ion channel proteins (15–18). MEC-6 primarily resides in the ER and is required for the proper folding, assembly, and surface expression of MEC-4 (19). Loss-of-function mutations of MEC-6 abolished both the mechanoreceptor current evoked by external forces as well as the worm's response to gentle touch, probably a result of defects in MEC-4 expression (13, 20).

The ENaC/degenerin family encodes a group of structurally related ion channels that participate in a large variety of fundamental physiological processes, such as mechanosensation, locomotion, nociception, fear-related behavior, seizure termination, detection of pheromones, airway fluid clearance, salt sensation, and extracellular Na^+ homeostasis (18, 21). ENaC mediates the rate-limiting step of Na^+ uptake across the apical membrane of specific epithelia. ENaC-dependent Na^+ absorption in the kidney plays important roles in regulating extracellular fluid volume and blood pressure as well as serum $[K^+]$ by facilitating renal K^+ secretion. ENaC-dependent Na^+ absorption in the airway also plays an important role in regulating airway surface liquid volume and mucociliary clearance (22). Functional ENaC complexes in the kidney consist of three

This work was supported, in whole or in part by National Institutes of Health Grants DK103834 (to S. S.) DK090195 (to T. M. B.), GM075061 (to J. L. B.), GM030997 (to M. C.), DK051391 (to T. R. K.), and DK079307 (Pittsburgh Center for Kidney Research). The authors declare that they have no conflicts of interest with the contents of this article. The content is solely the responsibility of the authors and does not necessarily represent the official views of the National Institutes of Health.

[1] To whom correspondence should be addressed: Renal-Electrolyte Division, University of Pittsburgh, 3550 Terrace St., Pittsburgh, PA 15261. Tel.: 412-647-3121; E-mail: kleyman@pitt.edu.

[2] The abbreviations used are: PON, paraoxonase; mPON, mouse PON; CCD, cortical collecting duct; ENaC, epithelial Na^+ channel; mENaC, mouse ENaC; ER, endoplasmic reticulum; HBS, Hepes-buffered saline; LSS, laminar shear stress; MBS, modified Barth's solution; P_o, open probability; ROMK, renal outer medullary potassium channel; ANOVA, analysis of variance.

homologous subunits, α, β, and γ, which form a trimeric ion channel (23). Each subunit contains a highly organized large extracellular domain, two transmembrane helices, and short cytosolic N and C termini (24–26). Like many other membrane-spanning proteins, this trimeric channel complex inefficiently assembles and folds in the ER, and thus only a small fraction of newly synthesized ENaC subunits exit the ER as assembled channels and traffic to the plasma membrane (27–29). Indeed, several molecular chaperones have been implicated in key steps during ENaC biogenesis, including subunit folding and channel assembly within the ER (30, 31). Other factors regulate intracellular trafficking, plasma membrane insertion, and retrieval as well as both ER-associated and lysosome-mediated degradation of ENaC (32–37). Together, this multistage machinery impacts the total number of channels (N) at the cell surface.

To date, it is unknown whether mammalian PON proteins regulate ion channel function. As MEC-6 functions as a molecular chaperone to facilitate the biogenesis of MEC-4/MEC-10 channels, we asked whether PON-2 regulates ENaC expression. We found that PON-2 is expressed in aquaporin 2 (AQP2)-positive principal cells of the distal nephron, where ENaC resides. PON-2 co-immunoprecipitated with ENaC subunits when expressed in HEK293 cells, and PON-2 reduces ENaC activity when expressed in oocytes. The PON-2–dependent reduction in ENaC activity is associated with a reduction in the number of Na^+ channels at the cell surface. Our data suggest that a conserved molecular chaperone has co-evolved with specific members of the ENaC/degenerin family to modulate ion channel expression.

Results

PON-2 is expressed in principal cells of the distal nephron

Deep RNA sequencing revealed that *pon-2* transcripts are present in most nephron segments of rat kidney, including collecting ducts (38). The presence of PON-2 protein has been reported in renal proximal tubules (10), but its presence in other nephron segments is less well-determined.

We evaluated the expression of PON-2 in human renal tubules by staining paraformaldehyde-fixed and cryopreserved human kidney sections with a rabbit polyclonal anti-human PON-2 antibody (Fig. 1*A*). As shown in Fig. 1*B*, the antibody recognizes two specific bands (~40 kDa) of the endogenous PON-2 in human whole kidney lysate as well as in mouse cortical collecting duct ($mCCD_{c1}$) cells overexpressing human PON-2. The antibody did not recognize endogenous mouse PON-2 in either the $mCCD_{c1}$ cells or mouse whole-kidney lysate (Fig. 1*B*), suggesting a high degree of species specificity. The human kidney sections were co-stained for AQP2, a marker for principal cells of the latter aspects of the distal nephron (39). We detected tubule-specific staining of PON-2 in human kidneys. PON-2 is detected in multiple nephron segments, including the AQP2-positive tubules (Fig. 1*A*). Notably, PON-2 (*red*) co-localized with AQP2 (*green*) in principal cells within the vicinity of the apical membrane (Fig. 1*A*). In addition, PON-2 was also detected in intercalated cells (which were negative for AQP2 staining) of the CCD (Fig. 1*A*). These results

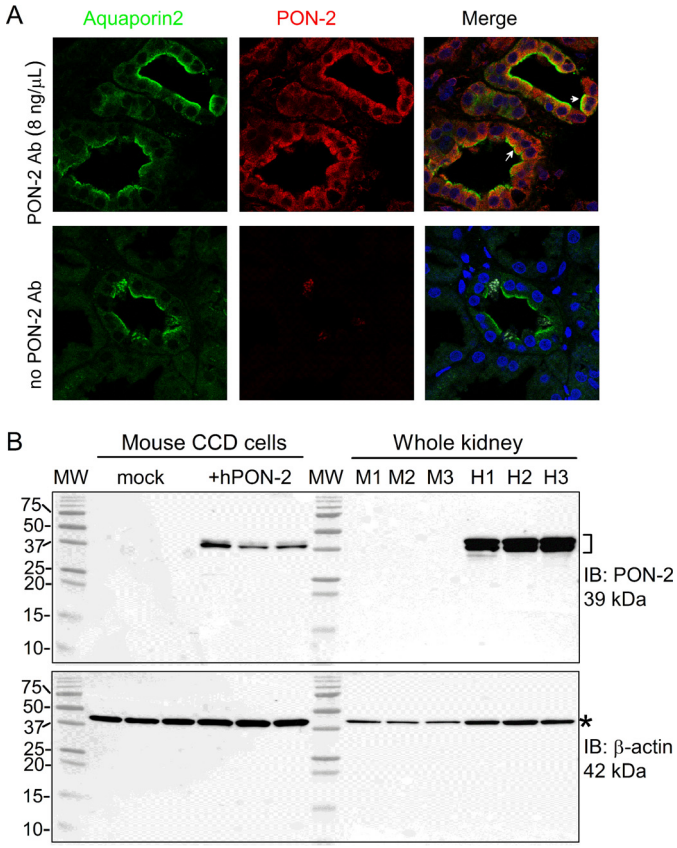

Figure 1. PON-2 is expressed in the aldosterone-sensitive distal nephron. *A*, human kidney sections were co-stained for PON-2 (*red*) and for AQP2 (*green*), a marker for principal cells of the aldosterone-sensitive distal nephron. Nuclei were stained with To-Pro3. The co-localization of PON-2 and AQP2 within collecting tubules is indicated by *arrows* in the *overlay image*. No PON-2 antibody (*Ab*) controls are shown with images taken under the same conditions. Experiments were performed with samples from three adult human kidneys. *B*, PON-2 antibody characterization. We assessed antibody specificity in $mCCD_{c1}$ cells transiently transfected with human PON-2 and control $mCCD_{c1}$ cells. This antibody recognized two bands around 40 kDa (the predicted size for PON-2) in $mCCD_{c1}$ cells expressing human PON-2. Additionally, the antibody recognized endogenous PON-2 protein in the whole human kidney lysate but not mouse kidney lysate. Blot were stripped and blotted for β-actin as loading control (denoted with an *asterisk*). The immunoblots (*IB*) were performed three times.

suggest that PON-2 is expressed in the distal nephron, where ENaC resides.

PON-2 interacts with ENaC subunits

AS PON-2 is expressed in principal cells of the distal nephron, we examined whether PON-2 is in a complex with ENaC subunits. Mouse PON-2 and V5 epitope–tagged mouse ENaC subunits were expressed in HEK293 cells. Each ENaC subunit (α, β, or γ) was individually expressed. Alternatively, the three subunits were co-expressed, with only one subunit bearing an epitope tag. Whole-cell lysates were immunoprecipitated with an anti-V5 antibody, and immunoblots were analyzed for the presence of PON-2 and ENaC subunits. As shown in Fig. 2, three ~40-kDa species of mouse PON-2 were detected in V5 precipitates as well as in whole-cell lysates (*top*). No co-immunoprecipitating proteins were observed in mock-transfected controls or when HEK293 cells were transfected with PON-2 alone. Mouse PON-2 co-immunoprecipitated with each of the three ENaC subunits when all three ENaC subunits

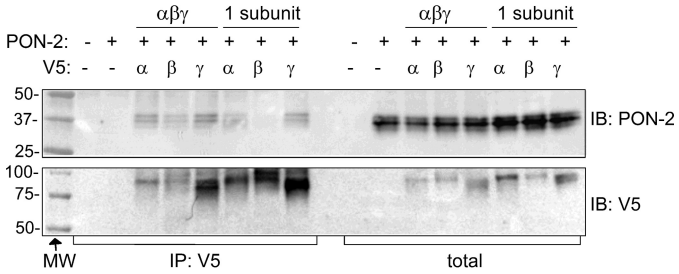

Figure 2. PON-2 co-immunoprecipitates with ENaC. Mouse PON-2 and mouse ENaC subunits were co-expressed in HEK293 cells as indicated. A C-terminal V5 epitope–tagged ENaC subunit (α, β, or γ) was expressed alone (single subunit) or with the other two untagged subunits to produce $\alpha\beta\gamma$ channels. Cell extracts were immunoprecipitated with anti-V5 antibodies. Both the immunoprecipitates (*IP*) (*left*) and total cell lysate (*right*) were subjected to SDS-PAGE and immunoblotting (*IB*) with either an anti-mouse PON-2 antibody (*top*) or the V5 antibody (*bottom*). The experiment was performed under non-reducing conditions (no β-mercaptoethanol in the sample buffer). The mobility of the Bio-Rad molecular weight standards (*MW*) is shown to the *right* of all blots. Three independent experiments were performed for each condition.

were present in the channel complex. In contrast, when PON-2 was co-expressed with individual ENaC subunits, the interaction between PON-2 and the β subunit was much weaker than with the α or γ subunit of ENaC (*top*), although the immunoprecipitation of β subunit was as efficient as that of the other two subunits (*bottom*). The expression of mouse PON-2 and ENaC subunits was detected in whole-cell lysates as expected (Fig. 2). We did not observe cleavage products of α and γ subunits, as the experiments were performed under non-reducing conditions, and the cleaved products are linked by a disulfide bond and will migrate with non-cleaved α and γ subunits (24–26).

PON-2 inhibits ENaC activity in oocytes

MEC-6 dramatically increased the activity of MEC-4/MEC-10 channels when expressed in *Xenopus* oocytes, probably by increasing channel surface expression (11, 19). If PON-2 is functionally related to MEC-6, we predicted that PON-2 expression would modify ENaC activity, perhaps via conserved mechanisms. To this end, we examined the effect of mouse PON-2 on mouse ENaC activity in *Xenopus* oocytes. Amiloride-sensitive Na^+ currents were readily detected in oocytes expressing ENaC (-1.5 ± 1.2 μA (mean $\pm$ S.D.), $n = 45$; Fig. 3, *A* and *B*). Surprisingly, co-expression of mouse PON-2 inhibited ENaC currents by $57 \pm 30\%$ (-0.7 ± 0.3 μA, $n = 51$, $p < 0.001$; Fig. 3, *A* and *B*), in contrast to the augmenting effect of MEC-6 on MEC-4/MEC-10 activity (11). Human PON-2 also elicited a similar effect on mouse ENaC activity ($41 \pm 46\%$ reduction in amiloride-sensitive Na^+ currents, $p < 0.001$; Fig. 3*C*), suggesting that the function of PON-2 on ENaC activity is conserved between mammalian species. The inhibitory effect of PON-2 is specific to ENaC, as PON-2 co-expression did not alter the activity of the renal outer medullary K^+ channel (ROMK) in oocytes (Fig. 3*D*). Co-injecting oocytes with cRNAs encoding mouse ENaC (2 ng cRNA/subunit) with increasing amounts of human *PON-2* cRNA (0, 0.4, 2, and 10 ng) was associated with a dose-dependent reduction in amiloride-sensitive Na^+ currents (Fig. 3*E*). We observed minimal whole-cell amiloride-insensitive currents in oocytes

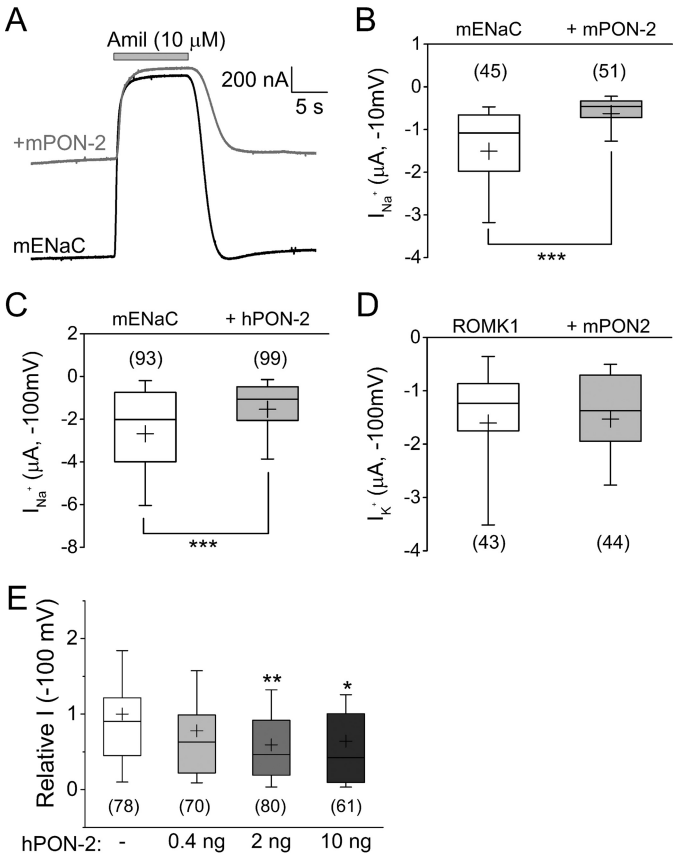

Figure 3. PON-2 inhibits ENaC expression in *Xenopus* oocytes. *A*, representative traces of whole-cell Na^+ current measured in oocytes expressing mouse ENaC (mENaC; 2 ng of cRNA/subunit) alone or co-expressing mouse PON-2 (+mPON-2, 2 ng of cRNA), with the holding potential set at -100 mV. After reaching a steady current, 10 μM amiloride (*gray bar*) was added to the bath. *B*, summary of the amiloride-sensitive Na^+ currents of mouse ENaC expressed alone or in the presence of mouse PON-2. Data were pooled from three batches of oocytes. *C*, summary of amiloride-sensitive Na^+ currents of mouse ENaC alone or co-expressed with human PON-2. Data were pooled from five batches of oocytes. *D*, summary of the $BaCl_2$-sensitive K^+ currents of oocytes expressing ROMK alone or ROMK with mouse PON-2. Data were pooled from three batches of oocytes. *E*, dose-dependent effect of PON-2 on ENaC activity. Oocytes were injected with mouse ENaC cRNAs alone (2 ng/subunit) or co-injected with the indicated amount of human *PON-2* cRNA (0.4, 2, or 10 ng). Whole-cell Na^+ currents were measured 24 h after injection at -100 mV. Data were pooled from four batches of oocytes. The average whole-cell Na^+ current in oocytes expressing ENaC alone was -2.1 ± 1.8 μA ($n = 78$). Statistical comparisons were analyzed with the unpaired Student's *t* test (*B–D*) (***, $p < 0.001$) or with one-way ANOVA followed by a Bonferroni's post hoc test (*E*) (*, $p < 0.05$; ** $p < 0.01$). The numbers of oocytes (*n*) assayed are indicated in each *panel*. *Whiskers*, 10th and 90th percentiles. +, mean.

injected with 10 ng of *PON-2* cRNA alone (-0.02 ± 0.04 μA, $n = 17$). In contrast, injection of large amounts (>10 ng) of MEC-6 cRNA alone produced large amiloride-insensitive currents in oocytes (11).

PON-2–dependent ENaC inhibition does not depend on its lactonase activity

PON-2 has a short cytoplasmic N terminus followed by a single transmembrane domain and a large C-terminal enzymatic domain that resides within the lumen of intracellular secretory organelles or in the extracellular space (6). The resolved structure of rabbit PON-1 resembles a six-bladed β-propeller with two calcium atoms in its central tunnel (12). Previous studies have shown that the conserved calcium-bind-

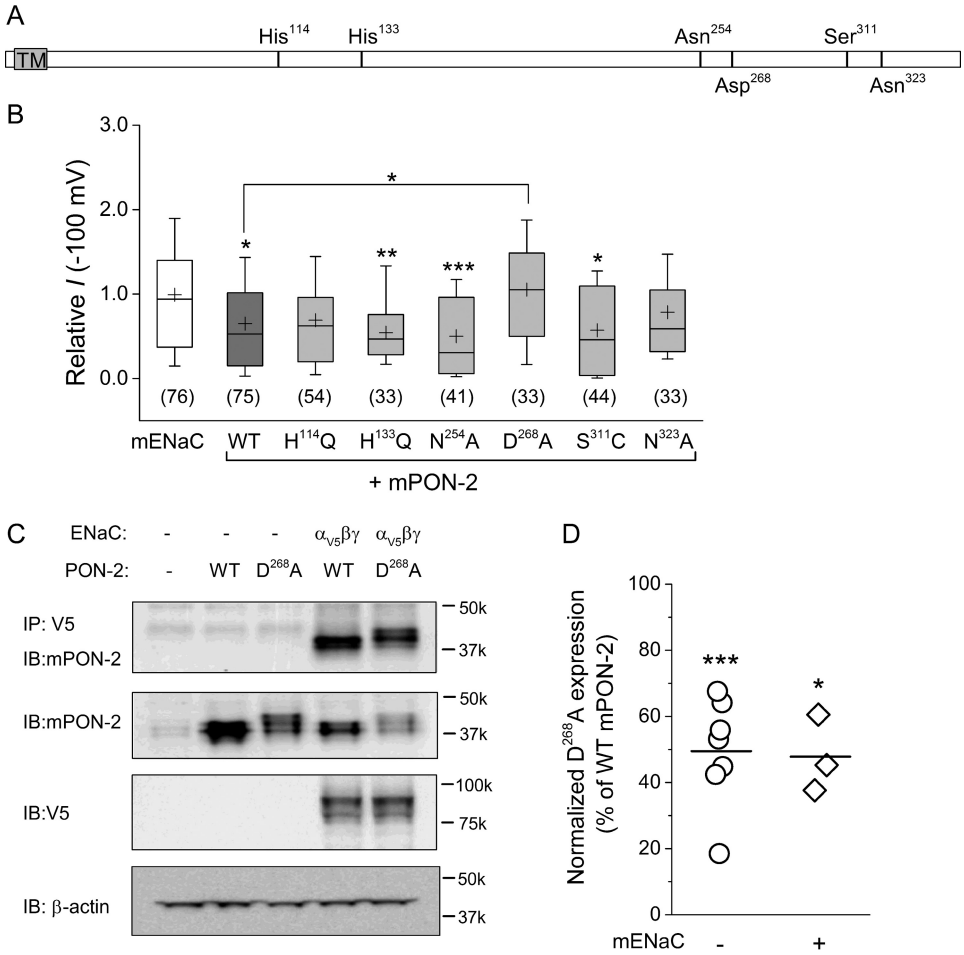

Figure 4. Key residues within PON-2 are not required for ENaC inhibition. *A*, a linear map of mouse PON-2, showing key residues required for enzymatic activity (His^{114}, His^{133}, and Asp^{268}) and *N*-glycosylation (Asn^{254} and Asn^{323}) as well as a common polymorphism (Ser^{311}). *B*, *Xenopus* oocytes were injected with cRNAs encoding mouse ENaC (2 ng/subunit) in the presence or absence of the cRNA (2 ng) of an individual PON-2 construct. Amiloride-sensitive Na^+ currents measured in individual oocytes were normalized to the average whole-cell Na^+ current of oocytes expressing mENaC alone from the same batch. The overall average whole-cell Na^+ current in oocytes expressing mouse ENaC alone was -3.4 ± 2.7 μA (*open bar*, $n = 76$). Data were collected from two batches of oocytes for each PON-2 mutant and four batches of oocytes for mENaC alone or mENaC plus WT PON-2. The numbers of oocytes (*n*) assayed are indicated in *parentheses*. *Whiskers*, 10th and 90th percentiles. +, mean. Statistical comparisons were analyzed with one-way ANOVA followed by a Bonferroni post hoc test (*, $p < 0.05$; **, $p < 0.01$; ***, $p < 0.001$). *C*, HEK293 cells were transfected with mouse PON-2 (WT or D268A) alone or co-transfected with mouse ENaC containing a C-terminal V5 epitope–tagged α subunit and non-tagged β and γ subunits, as indicated. Cell extracts were incubated with anti-V5 antibodies, and immunoprecipitates (*IP*) were immunoblotted (*IB*) with anti-PON-2 antibodies (*top*). Whole-cell lysates were immunoblotted with anti-PON-2 antibodies, anti-V5 antibodies, or anti-β-actin antibodies. SDS-PAGE was performed under non-reducing conditions. The mobility of the Bio-Rad molecular weight standards is shown to the *right* of the blots. *D*, PON-2 expression was normalized to the β-actin level in each experiment. The expression of the D268A mutant relative to WT PON-2 was assessed in seven or three independent experiments, respectively. *Bar*, mean. Statistical comparisons were analyzed with an unpaired Student's *t* test (*, $p < 0.05$; ***, $p < 0.001$).

ing sites within PON-2 (His^{114}, His^{133}, and Asp^{268}) are essential for its lactonase activity (40). In addition, there are two *N*-glycosylation sites (Asn^{254} and Asn^{323}) that are required for PON-2 maturation and activity (40, 41). To identify key sites within PON-2 that mediate its inhibitory effect on ENaC activity, we introduced single mutations at specific sites: H114Q, H133Q, D268A, N254A, and N323A (see Fig. 4*A*). In our experiments, we also introduced a Cys at Ser^{311}, which represents the most common PON-2 polymorphism (42). Whole-cell Na^+ currents were measured in oocytes expressing mouse ENaC alone or mouse ENaC plus either wild-type mouse PON-2 or an individual PON-2 mutant. The inhibitory effect of PON-2 on ENaC activity was retained with the H133Q, N254A, and S311C mutants (Fig. 4*B*). ENaC currents in oocytes expressing the H114Q and N323A mutants also appeared to be reduced, although the reductions in current did not reach statistical significance. In contrast, the PON-2 D268A mutant did not inhibit ENaC activity.

We next examined whether the lack of an inhibitory effect of the D268A mutant was due to impaired interaction between ENaC subunits and the PON-2 mutant. ENaC containing a V5-tagged α subunit was expressed in HEK293 cells with either wild-type mouse PON-2 or the D268A mutant. Both wild-type and D268A PON-2 co-immunoprecipitated ENaC (Fig. 4*C*), suggesting that the interaction between the channel complex and PON-2 was unaffected by the D268A mutation. We noticed that the expression level of the D268A mutant in HEK293 whole-cell lysates was lower than that of wild-type PON-2 ($49 \pm 16\%$ of wild-type PON-2, $n = 7$, $p < 0.001$ when expressed alone or $48 \pm 12\%$ of wild-type PON-2, $n = 3$, $p < 0.05$ when co-expressed with ENaC; Fig. 4*D*). These observations suggest that the loss of the inhibitory effect seen with the

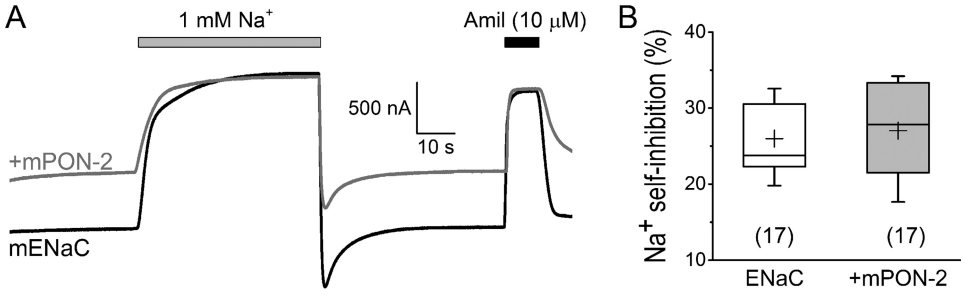

Figure 5. ENaC Na^+ self-inhibition is unaffected by PON-2. *A*, superimposed traces from oocytes expressing mENaC (*black*) or co-expressing mPON-2 (*gray*) are shown. At $t = 70$ s, the bath perfusion with 1 mM Na^+ (*gray bar*) was switched to 110 mM Na^+ to initiate the Na^+ self-inhibition response. Amiloride was added to the bath at the end of each recording (*black bar*). *B*, the percentage of channel inhibition by extracellular Na^+ was estimated as described under "Experimental procedures." Data were pooled from three experiments using different batches of oocytes. The numbers of oocytes (*n*) assayed are indicated in *parentheses*. *Whiskers*, 10th and 90th percentiles. +, mean. No statistical significance was found between the two groups with an unpaired Student's *t* test.

PON-2 D268A mutant may reflect decreased PON-2 protein expression.

PON-2 does not affect ENaC gating in response to extracellular factors

The inhibitory effect of PON-2 on ENaC activity suggests a reduction in channel open probability (P_o) and/or in the number (N) of functional channels at the cell surface. ENaC activity is tightly regulated by a variety of endogenous or external factors that affect channel biogenesis or gating (43, 44). Inhibition of ENaC by extracellular Na^+ and activation of ENaC by laminar shear stress (LSS), a mechanical force, both reflect changes in channel P_o (45–47). To investigate whether PON-2 inhibits ENaC activity by affecting channel gating, we examined the Na^+ self-inhibition response of mouse ENaC in oocytes in the presence or absence of PON-2 (Fig. 5). A rapid increase in bath [Na^+] from 1 to 110 mM resulted in a 26 ± 5% reduction in the whole-cell steady-state current, relative to the peak current in oocytes expressing ENaC alone (Fig. 5*B*). We observed a similar degree of current reduction in oocytes co-expressing mouse PON-2 (27 ± 6% (Fig. 5*B*)). We also examined the LSS response of ENaC by exposing oocytes to flow-mediated shear stress delivered through vertical perfusion (Fig. 6). LSS of 0.12 dynes/cm^2 evoked a 2.2 ± 0.5-fold increase in whole-cell Na^+ currents in oocytes expressing ENaC alone (Fig. 6*B*). The co-expression of PON-2 with ENaC did not change the magnitude of the LSS response (2.0 ± 0.5 increase in Na^+ currents; Fig. 6*B*).

ENaC activation by an exogenous protease is unaffected by PON-2

Both the α and γ subunits of ENaC are cleaved by proteases (48, 49). Proteases, such as trypsin and chymotrypsin activate ENaC by releasing embedded inhibitory tracts, thus increasing channel P_O at the cell surface (50–53). This phenomenon allows for a measure of whether a protein or condition affects channel density (N) or P_O at the plasma membrane. α-chymotrypsin treatment (2 μg/ml for 2 min) increased whole-cell Na^+ currents by 1.9 ± 0.6-fold in oocytes expressing mouse ENaC (Fig. 7). We observed a similar activating effect of α-chymotrypsin in oocytes co-expressing ENaC and PON-2 (1.8 ± 0.9-fold increase in whole-cell Na^+ currents (Fig. 7*B*)). As ENaC activity was still lower in the presence of PON-2 after α-chymotrypsin treatment (52 ± 27% reduction, $p < 0.001$), our results suggest that ENaC density at the cell surface in oocytes was reduced by PON-2. In summary, the effects of several factors that regulate ENaC P_o are not altered by PON-2.

PON-2 reduces ENaC surface expression

To definitively establish that PON-2 reduces ENaC expression at the cell surface, we examined ENaC surface expression in oocytes using channels with a β subunit bearing an external FLAG epitope in conjunction with a chemiluminescence-based assay, as described previously (54). Surface expression of wild-type channels (non-FLAG-tagged), expressed as relative light units, was $0.1 \pm 0.1 \times 10^6$ ($n = 29$) but rose to $2.3 \pm 2.3 \times 10^6$ when ENaC bearing the external FLAG epitope was expressed ($n = 42$; Fig. 8*A*). Notably, this value was significantly reduced in oocytes co-expressing PON-2 ($0.9 \pm 0.9 \times 10^6$, $n = 50$, $p < 0.001$). Furthermore, the PON-2–dependent reduction in ENaC surface expression (63 ± 60%; Fig. 8*A*) was similar in magnitude to the PON-2-dependent reduction in ENaC current (57 ± 30%; Fig. 3*B*). In contrast, whole-cell expression of both full-length and cleaved α ENaC in oocytes was not altered by the co-expression of mouse PON-2 (Fig. 8, *B* and *C*).

Functional conservation between PON-2 and MEC-6

MEC-6 and POML-1, two PON-2 orthologues found in *C. elegans*, enhanced MEC-4/MEC-10 channel expression in oocytes (11, 19), whereas our results showed that PON-2 inhibited ENaC expression (Fig. 3). Therefore, we examined whether the functional properties regarding ion channel regulation among members of this structurally related family are conserved. To test this, we injected oocytes with cRNAs encoding mouse ENaC with or without MEC-6 cRNA. As shown in Fig. 9*A*, the average amiloride-sensitive Na^+ current in oocytes co-expressing MEC-6 (−0.5 ± 0.6 μA, $n = 64$) was significantly lower than oocytes expressing only mouse ENaC (−1.5 ± 1.7 μA, $n = 68$, $p < 0.001$), suggesting that like PON-2 (see Fig. 3), MEC-6 also inhibits ENaC activity. We also examined whether PON-2, like MEC-6, affects the activity of MEC-4/MEC-10 channels. Whereas the activity of MEC-4/MEC-10 channels was significant enhanced by MEC-6, it was unaltered by mouse PON-2 (Fig. 9*B*).

Discussion

PON-2 shares structural features with MEC-6, an ER-resident chaperone in *C. elegans* that enhances the biogenesis of MEC-4/MEC-10 channels in worms (19). In this paper, we

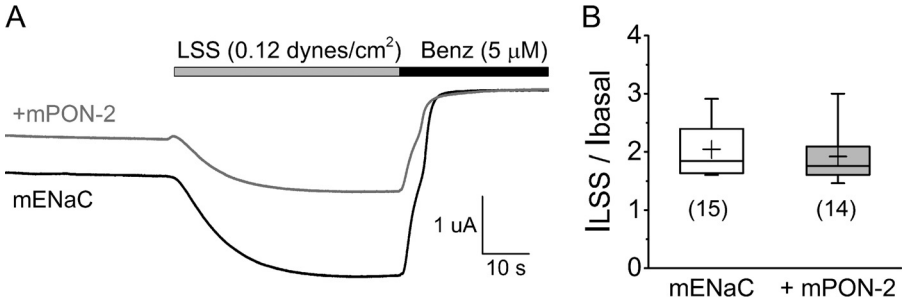

Figure 6. PON-2 does not alter LSS-mediated ENaC activation. *A*, superimposed traces of LSS-mediated activation of mENaC (*black*) or mENaC + mPON-2 (*gray*). A vertical flow rate of 1.5 ml/min was initiated at $t = 35$ s to apply LSS (*gray bar*). At the end of the experiment, 5 μM benzamil was added to the bath (*black bar*). *B*, the magnitude of channel activation by LSS was estimated as described under "Experimental procedures." Data were pooled from three experiments using different batches of oocytes. The number of oocytes (*n*) assayed is indicated in *parentheses*. *Whiskers*, 10th and 90th percentiles; +, mean. No statistical significance was found between the two groups with an unpaired Student's *t* test.

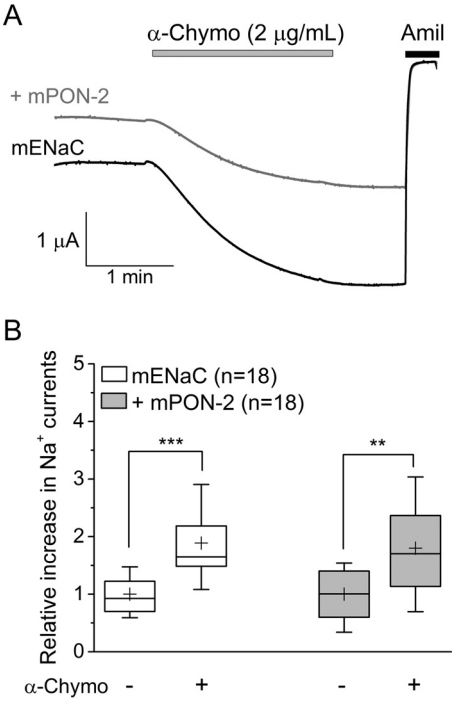

Figure 7. PON-2 does not affect the magnitude of ENaC activation by α-chymotrypsin. *A*, superimposed traces from oocytes expressing mENaC (*black*) or co-expressing mPON-2 (*gray*). α-Chymotrypsin (2 μg/ml) was added to oocytes for 2 min (*gray bar*) to reach the peak current, followed by 1-min perfusion with the bath solution. Amiloride was added to the bath at the end of each recording (*black bar*). *B*, relative increase in whole-cell Na^+ currents in response to α-chymotrypsin treatment. Whole-cell Na^+ currents were measured prior to (−) and following (+) α-chymotrypsin treatment in individual oocytes. The relative increases in whole-cell Na^+ currents were estimated by normalizing the basal currents prior to stimulation by α-chymotrypsin in the same oocyte. The average basal current (prior to the α-chymotrypsin treatment) was 1.9 ± 1.5 μA in oocytes expressing mENaC and 1.1 ± 1.3 μA in oocytes co-expressing mENaC and mPON-2. Data were pooled from four experiments using different batches of oocytes. The numbers of oocytes (*n*) assayed are indicated in the graph. *Whiskers*, 10th and 90th percentiles; +, mean. Statistical comparisons were analyzed with two-way ANOVA followed by a Bonferroni post hoc test (**, $p < 0.01$; ***, $p < 0.001$).

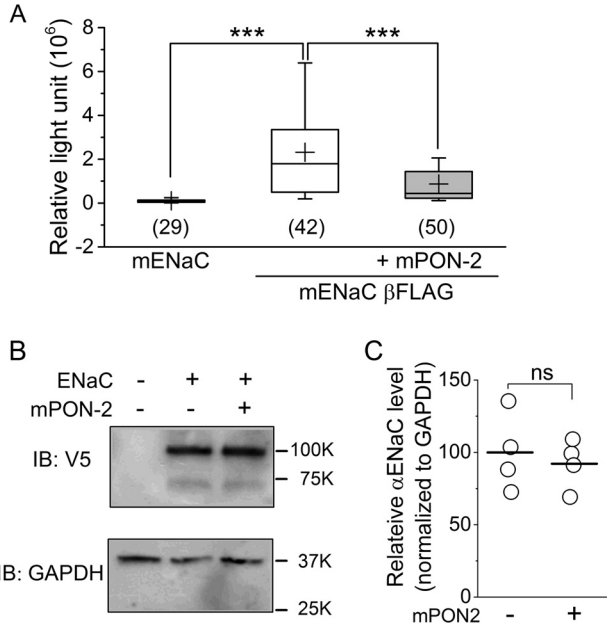

Figure 8. PON-2 reduces ENaC cell surface expression in *Xenopus* oocytes. *A*, oocytes were injected with 2 ng of cRNA/subunit of mENaC (lacking a FLAG tag), mENaC with a FLAG-tagged β subunit (mENaC βFLAG), or mENaC βFLAG + mouse PON-2 at a cRNA ratio of 1:1. Surface expression of ENaC was measured 48 h after injection and is shown as the average of relative light units from individual oocytes. Data were pooled from three independent experiments using different batches of oocytes. The numbers of oocytes (*n*) assayed are indicated in the graph. *Whiskers*, 10th and 90th percentiles; +, mean. Statistical comparisons were analyzed with one-way ANOVA followed by a Bonferroni post hoc test (***, $p < 0.001$). *B*, *Xenopus* oocytes were injected with 2 ng of cRNA/subunit of mENaC containing a V5-tagged α subunit alone or co-injected with an equal amount of mouse PON-2 cRNA. An equal number of non-injected oocytes were used as a negative control. The following day, oocytes were homogenized and immunoblotted (*IB*) with either an anti-V5 antibody or an anti-GAPDH antibody. The mobility of the Bio-Rad molecular weight standards is shown to the *right* of the immunoblots. *C*, ENaC α subunit expression (full-length polypeptide + cleavage product) was normalized to the GAPDH level in each experiment. The effect of PON-2 on α subunit expression was assessed in four independent experiments. *Bar*, mean. No significant changes were observed in α subunit expression when analyzed with an unpaired Student's *t* test.

examined whether PON-2 plays a role in regulating ENaC, an ion channel that is structurally related to the MEC-4/MEC-10 channel.

ENaC subunits are expressed in the latter aspect of the aldosterone-sensitive distal nephron, a key site for the highly regulated reabsorption of filtered Na^+ as well as tubular K^+ secretion (55). We found that PON-2 is expressed in AQP2-positive principal cells in the distal nephron of human kidney. It is also expressed in AQP2-negative intercalated cells of the distal nephron as well as other nephron segments (*e.g.* AQP2-negative tubules). This finding is not surprising, as *pon-2* transcripts were detected in multiple segments of the rat nephron (38), and PON-2 protein expression has been reported in mouse and human proximal tubules (10).

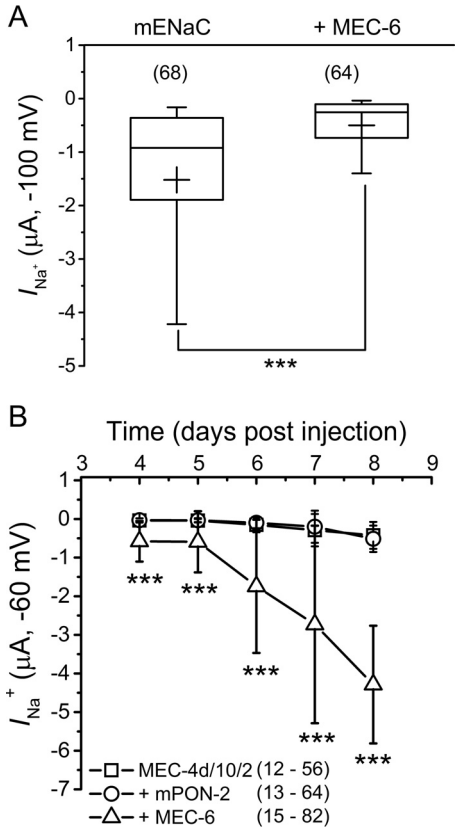

Figure 9. Effects of MEC-6 on ENaC activity and of PON-2 on MEC-4/MEC-10 activity. *A*, whole-cell Na^+ currents were measured in oocytes expressing mouse ENaC (2 ng cRNA/subunit) alone or co-expressing MEC-6 (2 ng of cRNA) 24 h after cRNA injection at a holding potential of −100 mV. Amiloride (10 μM) was added to the bath to determine leak currents at the end of each recording. The numbers of oocytes (*n*) assayed for each group are indicated in *parentheses*. *Whiskers*, 10th and 90th percentiles; +, mean. Statistical comparison was analyzed with an unpaired Student's *t* test (***, $p < 0.001$). *B*, oocytes were injected with cRNAs encoding MEC-4 A713T, MEC-10, and MEC-2 (5 ng/each) alone or with the addition of cRNA (1 ng) encoding either MEC-6 or mouse PON-2. Whole-cell Na^+ currents were measured 4–8 days after cRNA injection by clamping oocytes at −60 mV. At the end of each recording, 50 μM benzamil was added to the bath to determine leak currents. The experiment was performed with four individual batches of oocytes. For the latter time points, data were pooled from at least two batches of oocytes. Results were expressed as the mean ± S.D. with the numbers of oocytes (*n*) assayed indicated in *parentheses*. Statistical comparisons of benzamil-sensitive whole-cell currents of oocytes injected with MEC-4 A713T, MEC-10, and MEC-2 *versus* MEC-4 A713T, MEC-10, and MEC-2, and either MEC-6 or mouse PON-2 at each time point was analyzed with one-way ANOVA followed by a Bonferroni post hoc test (***, $p < 0.001$).

We found that PON-2 and ENaC subunits are components of a protein complex when co-expressed in HEK293 cells (Fig. 2). Mouse PON-2 co-immunoprecipitated each mouse ENaC subunit when all three ENaC subunits were co-expressed in HEK293 cells. When individual mouse ENaC subunits were expressed in HEK293 cells, the α and γ subunits co-immunoprecipitated with mouse PON-2. Weak co-immunoprecipitation was seen with the β subunit. These subunit-specific ENaC/PON-2 interactions suggest that conformational differences exist among ENaC subunits that depend on whether one or three ENaC subunits are expressed, which in turn impacts interactions within the complex. Functional ENaCs comprise subunits that are 30–40% identical at the amino acid level. Subunit-specific interactions have also been shown with ENaC and Lhs1/GRP170, an ER-resident Hsp70-like chaperone protein (33). Lhs1/GRP170–mediated ENaC degradation was specific for the α subunit expressed alone and was blocked when the other two subunits were present in the channel complex (33, 56). Nonetheless, our data show that PON-2 interacts with ENaC subunits in a heterologous expression system and raise the possibility that these interactions occur in the distal nephron and perhaps in other epithelia.

MEC-6 functions as a chaperone, increasing MEC-4/MEC-10–dependent whole-cell Na^+ currents when expressed in *Xenopus* oocytes (11, 19). Interestingly, PON-2 did not alter MEC-4/MEC-10 currents in oocytes. In contrast, both PON-2 and MEC-6 reduced ENaC currents in oocytes (Figs. 3 and 9). Our observations suggest that the chaperone function of *C. elegans* and mammalian paraoxonase-like proteins is conserved, although they have distinct effects on different members of the ENaC/degenerin ion channel family.

It is well-known that chaperones exert different effects on functionally related proteins, and their effects may be cell type–specific. For example, whereas Hsc70 enhances ASIC2 expression in vascular smooth muscle cells (57), it reduces ASIC2 expression in glioma cells as well as ENaC expression in Madin–Darby canine kidney cells (35, 58). The adaptability of molecular chaperones is well-documented (59). For example, homologous Hsp90α and Hsp90β have different effects on endothelial nitric oxide signals (60). Moreover, the related heat shock proteins, Hsc70 and Hsp70, exert different effects on ENaC expression (34). Even minor changes in a chaperone substrate (in many cases a single missense mutation) can dramatically affect substrate specificity and chaperone function (61).

It has been shown that PON-2 lactonase activity is impaired by mutating the calcium-binding sites (His^{114}, His^{133}, and Asp^{268}) or residues that impact protein maturation (Asn^{254} and Asn^{323}) (40, 41). To determine whether the lactonase activity of PON-2 is required for ENaC regulation, we introduced mutations at these sites in mouse PON-2 (Fig. 4*A*). The reduction in ENaC activity observed with both wild-type PON-2 and some mutants (H133Q, N254A, and S311C) was significant (Fig. 4*B*). For other mutants, reductions in ENaC currents were also evident but did not achieve significance (H114Q and N323A). There was only one mutant (D268A) where we observed levels of functional ENaC expression that were similar to levels seen with ENaC alone (*i.e.* in the absence of PON-2). Whole-cell expression levels of the PON-2 D268A mutant were ~50% of wild-type PON-2 (Fig. 4*D*). The reduced expression levels of this mutant could explain the lack of an inhibitory effect of the D268A mutant on ENaC activity. Assuming that these mutants result in a loss of PON-2 lactonase activity (40, 41), our results suggest that lactonase activity is dispensable for PON-2–dependent inhibition of ENaC.

ENaCs are exposed to multiple extracellular factors, including ions, proteases, and mechanical forces, which regulate channel activity by altering P_o, (44, 53). We examined whether PON-2 affects ENaC gating in response to these extracellular stimuli. The relative magnitude of ENaC activation by LSS or chymotrypsin was unaffected by PON-2 (Figs. 6 and 7). Furthermore, the extent of channel inhibition by extracellular Na^+ was unaffected by PON-2 (Fig. 5). Together, these data suggest that PON-2 does not alter the regulation of ENaC P_o by these

factors. These results are also consistent with our findings that reduced ENaC activity by PON-2 reflects reduced channel density at the cell surface (Fig. 8) and suggest that PON-2 modifies ENaC biogenesis and/or intracellular trafficking.

PON-2 can counteract lipid peroxidation at the plasma membrane (6). Under oxidative stress, endogenous PON-2 is recruited to the plasma membrane and protects the membrane from lipid peroxidation (6). ENaC subunits comprise two membrane-spanning domains and are believed to interact with membrane phospholipids as well as membrane-anchored proteases, which then modulate channel activity (62–66). We cannot rule out the possibility that PON-2 might modify membrane lipid composition in the setting of oxidative stress and alter ENaC gating.

In summary, we identified PON-2 as a novel regulator of ENaC that acts by altering the number of channels at the cell surface. As ENaC performs critical functions in many epithelia, its regulation by molecular chaperones represents an essential checkpoint for ENaC quality control in health and disease.

Experimental procedures

Site-directed mutagenesis and in vitro transcription

Human *PON-2* was cloned in the pCDNA3.1 vector (a gift from Dr. Srinivasa T. Reddy, UCLA). Mouse *Pon-2* in the pCMV6 vector was purchased from OriGene (Rockville, MD). PON-2 mutants tested in the study were generated with a Q5 site-directed mutagenesis kit (New England Biolabs, Ipswich, MA). Nucleotide sequencing was performed to confirm the targeted mutations. cRNAs of mouse and human ENaC α, β, and γ subunits; mouse and human PON-2 constructs; or *C. elegans* MEC-2, MEC-4 A713T, MEC-6, and MEC-10 cRNAs were synthesized following the manufacturer's protocols with the T3 or T7 mMESSAGE mMACHINE, respectively (Thermo Fisher Scientific). Previously described ENaC subunits with an N-terminal HA epitope tag and a C-terminal V5 epitope tag (48) were used for detecting protein–protein interaction in HEK293 cells.

Oocyte expression and whole-cell current measurement

Oocytes were harvested from *Xenopus laevis* following a protocol approved by the University of Pittsburgh Institutional Animal Care and Use Committee. Stage V-VI oocytes were injected with 2 ng of cRNA/subunit of mouse ENaC or 1 ng of rat ROMK cRNA. Equal amounts of mouse or human PON-2 (or mutant mouse PON-2) cRNAs were injected for the co-expression assay, unless otherwise noted. The injected oocytes were incubated in modified Barth's saline (MBS: 88 mM NaCl, 1 mM KCl, 2.4 mM $NaHCO_3$, 15 mM HEPES, 0.3 mM $Ca(NO_3)_2$, 0.41 mM $CaCl_2$, 0.82 mM $MgSO_4$, 10 μg/ml sodium penicillin, 10 μg/ml streptomycin sulfate, and 100 μg/ml gentamycin sulfate, pH 7.4) at 18 °C. All experiments were performed at room temperature 24–48 h following injections. Oocytes were placed in a recording chamber from Warner Instruments (Hamden, CT) and perfused with a solution containing 110 mM NaCl, 2 mM KCl, 1.6 mM $CaCl_2$, and 10 mM HEPES, pH adjusted to 7.4 (NaCl-110). Voltage clamp was performed using a Dagan TEV-200 amplifier (Dagan Corp., Minneapolis, MN) and DigiData 1440A interface (Molecular Devices, Sunnyvale, CA). Whole-cell Na^+ currents were measured by clamping oocytes at −100 mV. To examine the effect of proteases on ENaC activity, oocytes were perfused with NaCl-110 containing 2 μg/ml α-chymotrypsin (C4879, Sigma) for 2 min. At the end of each recording, oocytes were perfused with 10 μM amiloride to determine ENaC-independent leak currents. To measure the PON-2 effect on ROMK activity, we replaced the NaCl in the perfusion solution with 100 mM KCl. Whole-cell K^+ currents were measured by clamping oocytes at −100 mV. At the end of each recording, 5 mM $BaCl_2$ was delivered to the oocyte to determine ROMK-independent leak currents (67). To examine *C. elegans* degenerin channel expression, oocytes were injected with cRNAs encoding MEC-4 A713T (MEC-4d, degenerin mutant), MEC-10, and MEC-2 (5 ng/each) alone or with the addition of cRNA (1 ng) encoding either MEC-6 or mouse PON-2. 4–8 days after cRNA injection, Na^+ currents were measured by clamping oocytes at −60 mV. At the end of each recording, 50 μM benzamil was added to the bath to determine leak currents.

LSS response assay

Oocytes were placed in a recording chamber (20-mm diameter and 6 mm deep) that was constantly perfused with the NaCl-110 solution at a rate of 3.5 ml/min. LSS of 0.12 dynes/cm^2 was applied by perfusion (1.5 ml/min) through a vertical pipette submerged near the top of the oocyte (68). A final concentration of 5 μM benzamil was added to the bath at the end of each experiment to determine the ENaC-independent leak current. The magnitude of the LSS response was expressed as a ratio between the LSS stimulated current (I_{LSS}) and the basal current (I_{basal}). When determining I_{LSS} and I_{basal}, whole-cell currents were corrected for the benzamil-insensitive component.

Na^+ self-inhibition assay

To measure the inhibition of ENaC by extracellular Na^+, oocytes were perfused with the NaCl-110 solution for the first 60 s and then with NaCl-1, a low-[Na^+] bath solution (NaCl-1) that contains 1 mM NaCl, 109 mM *N*-methyl-D-glucamine, 2 mM KCl, 1.6 mM $CaCl_2$, and 10 mM HEPES, pH adjusted to 7.4 with HCl for another 40 s. To initiate Na^+ self-inhibition, the NaCl-1 solution was rapidly replaced by the NaCl-110 solution while whole-cell currents were continuously recorded. At the end of each experiment, the oocyte was perfused with 10 μM amiloride prepared in NaCl-110. The maximal inward current immediately after the switch from NaCl-1 to NaCl-110 (I_{peak}) and the steady-state current (I_{ss}) measured 40 s after the I_{peak} were obtained to assess the percentage of current loss due to Na^+ self-inhibition. Whole-cell currents were corrected for the amiloride-insensitive component when determining I_{peak} and I_{ss}.

ENaC surface expression and whole-cell expression in oocytes

A chemiluminescence assay was performed to assess ENaC surface expression in oocytes as described previously (54). Mouse ENaC β subunit with an extracellular FLAG epitope tag (DYKDDDDK) was included in the cRNA mixture. A non-tagged wild-type β subunit was used as a control. Surface expression was assayed 2 days after cRNA injection. Briefly,

oocytes were initially incubated in MBS supplemented with 1% BSA (MBS-BSA, without antibiotics) for 30 min. Oocytes were then labeled with a monoclonal anti-FLAG M2 antibody (1 μg/ml; F3165, Sigma) in MBS-BSA for 2 h on ice. Following extensive wash with MBS-BSA, oocytes were incubated with an HRP-coupled goat anti-mouse IgG (1 μg/ml; 115036072, Jackson ImmunoResearch, West Grove, PA) in MBS-BSA for 1 h on ice. To remove excess antibodies, oocytes were extensively washed with MBS-BSA followed by MBS. Only intact oocytes were then transferred into a 96-well plate individually, and 100 μl of SuperSignal ELISA Femto maximum sensitivity substrates (Thermo Fisher Scientific) was added to each well. After incubation at room temperature for 1 min, the chemiluminescence of each oocyte was quantified as relative light units with a Glo-Max-Multi Detection System (Promega, Madison, WI).

ENaC whole-cell expression in the presence and absence of mouse PON-2 was assessed with Western blotting. Oocytes were injected with 2 ng of mouse ENaC cRNAs containing a V5-tagged α subunit with or without an equal amount of mouse PON-2 cRNA. 24 h after injection, 15–20 oocytes of each group were lysed in a detergent solution (100 mM NaCl, 40 mM KCl, 1 mM EDTA, 10% glycerol, 1% Nonidet P-40, 0.4% deoxycholate, 20 mM HEPES, pH 7.4) supplemented with protease inhibitor mixture III (Calbiochem). The homogenate was vortexed for 30 s and subsequently centrifuged at 200 $\times$ *g* and then 20,800 $\times$ *g* for 10 min at 4 °C. The supernatant (whole-cell lysate) was heated for 5 min at 95 °C with an equal amount of Bio-Rad Laemmli sample buffer containing 0.14 M β-mercaptoethanol and subjected to SDS-PAGE and immunoblotting with either the anti-V5 antibody (0.2 μg/ml; Invitrogen) or anti-GAPDH antibody (0.2 μg/ml, ProteinTech, Rosemont, IL). The immunoblots were developed using a chemiluminescence reagent (Pierce™ ECL Western blotting substrate, Thermo Fisher Scientific) and imaged with the Bio-Rad ChemiDoc™ system. Experiments were repeated in four batches of oocytes.

Co-immunoprecipitation of PON-2 and ENaC

HEK293 cells grown on 6-well size dishes were transfected with the indicated amount of plasmids encoding PON-2 and ENaC subunits using Lipofectamine 2000 (Invitrogen). An epitope-tagged ENaC subunit (+PON-2) was transfected alone or with non-tagged subunits to express $\alpha\beta\gamma$ ENaC. In each case, only one ENaC subunit had a C-terminal V5 epitope tag. The next day, cells were extracted with 0.25 ml of detergent solution (20 mM HEPES, 100 mM NaCl, 40 mM KCl, 1 mM EDTA, 10% glycerol, 1% Nonidet P-40, 0.4% deoxycholate, pH 7.4) supplemented with protease inhibitor mixture III (Calbiochem) for 10 min on ice. Insoluble material was removed by centrifugation at 14,000 rpm for 7 min at 4 °C, and a 5% aliquot of the supernatant was retained as a whole-cell lysate. The supernatant was incubated for 2 h at 4 °C with end-over-end mixing with 40 μl of anti-V5 antibodies conjugated to beads (Invitrogen). The isolated beads were washed once with HEPES-buffered saline (HBS: 10 mM HEPES, 150 mM NaCl with phosphatase inhibitors, pH 7.4) containing 1% Triton X-100 and then once with HBS before proteins were eluted into 30 μl of Laemmli sample buffer (Bio-Rad) by heating at 90 °C for 5 min. Both the immunoprecipitated and whole-cell lysate were subjected to immunoblotting by SDS-PAGE on a Bio-Rad Criterion 4–15% gel and transferred to Millipore nitrocellulose. The membrane was incubated with a rabbit anti-PON-2 antibody (1 μg/ml; ab40969, Abcam) overnight at 4 °C, followed by a 1-h incubation with an HRP-conjugated goat anti-rabbit antibody (KPL-474-1506, Gaithersburg, MD). The expression of V5-tagged ENaC subunits was detected in the whole-cell lysate by blotting the membranes with a mouse anti-V5 antibody (0.2 μg/ml; R96025, Invitrogen) overnight at 4 °C, followed by a 1-h incubation with an HRP-conjugated goat anti-mouse (KPL-474-1806). The immunoblots were developed using a chemiluminescence reagent (Pierce™ ECL Western blotting substrate, Thermo Fisher Scientific) and imaged with the Bio-Rad ChemiDoc™ system. Experiments were performed a minimum of three times.

Kidney tissue immunostaining and confocal microscopy

Adult human kidneys were obtained from fresh cadavers by the Center for Organ Recovery and Education (Pittsburgh, PA) through a protocol approved by the University of Pittsburgh Committee for Oversight of Research and Clinical Training Involving Decedents. Kidney transverse sections (5–10 mm) were fixed in 4% paraformaldehyde overnight at 4 °C, followed by three 15-min washes in cold PBS. Fixed tissues were quenched in 200 mM NH_4Cl for 15 min at 4 °C, followed by three 15-min washes with cold PBS, and stored in PBS with 0.02% NaN_3 at 4 °C. Fixed kidney wedges were soaked in 30% sucrose overnight at 4 °C and frozen by embedding in OCT medium at −20 °C. Kidney tissues were then cut into 4–5-μm sections on a Leica CM1950 cryostat. Tissues were stained using a SDS-mediated antigen retrieval method adapted from Brown *et al.* (69). Briefly, tissues were rehydrated in PBS and blocked with 1% BSA in PBS for 15 min. Slides were then incubated with a rabbit anti-human PON-2 antibody (8 μg/ml; ab183710, Abcam) and a goat anti-AQP2 antibody (0.2 μg/ml; sc-9882, Santa Cruz Biotechnology, Inc., Dallas, Texas) for 75 min at room temperature in a humid box. After extensive washes with PBS, slides were then incubated with secondary antibodies (donkey anti-rabbit Cy3 for PON-2 and donkey anti-goat FITC for AQP2) for 1 h at room temperature in a humid box. All antibody dilutions were performed in a background-reducing reagent (DAKO, Carpinteria, CA). Slides were then washed with PBS and covered with a droplet of To-Pro3 nuclear stain (0.33 μM) for 5 min. After washing twice in PBS, the slides were mounted on coverslips with VectaShield medium (Vector Laboratories, Burlingame, CA). Slides were imaged on a Leica TCS SP5 CW-STED confocal imaging system with a $\times$63 glycerol immersion lens with a 1.25 numerical aperture.

The specificity of the anti-PON-2 antibody (ab183710, Abcam) was validated by immunoblotting. $mCCD_{c1}$ cells were transiently transfected with the human PON-2 cDNA using Lipofectamine 2000 (Invitrogen). 24 h after transfection, cells were lysed directly in Laemmli sample buffer containing 0.14 M β-mercaptoethanol. Control non-transfected (mock) $mCCD_{c1}$ cells were also lysed for immunoblotting. Kidneys from three C57BL/6 mice and three human samples were individually homogenized in the detergent buffer in the presence of protease and phosphatase inhibitors. Both $mCCD_{c1}$ cell lysates and

whole-kidney lysates were subjected to SDS-PAGE under reducing conditions and blotted with the rabbit anti-PON-2 antibody (0.8 μg/ml; ab183710, Abcam) overnight at 4 °C, followed by a 1-h incubation with an HRP-conjugated goat anti-rabbit antibody (KPL-474-1506). The blot was then stripped and probed with a mouse anti-β-actin antibody (0.21 μg/ml; A1978, Sigma) overnight at 4 °C, followed by a 1-h incubation with an HRP-conjugated goat anti-mouse antibody (KPL-474-1806). Immunoblots were developed using a chemiluminescence reagent (Pierce™ ECL Western blotting substrate, Thermo Fisher Scientific) and imaged with the Bio-Rad ChemiDoc™ system.

Statistical analyses

Two-electrode voltage-clamping experiments were repeated with a minimum of two batches of oocytes obtained from different frogs, and the numbers of replicates are indicated in the figure legends. Data are expressed as the mean ± S.D. throughout. *Box-and-whisker diagrams* are used to show the distribution of data: median (*middle line*), mean (*cross*), 25th to 75th percentile (*box*), 10th to 90th percentile (*whisker*). The number of oocytes examined for each group is indicated in the figures. Electrophysiological data were analyzed with Clampfit version 10.5 and plotted with Origin 2015 (OriginLab, Northampton, MA). Statistical comparisons were made using Origin 2015. A p value of <0.05 was considered statistically significant.

Author contributions—M. C., J. L. B., and T. R. K. devised the project. S. S., T. R. K., R. P. H., T. M. B., and J. L. B. designed the experiments, analyzed data, and prepared the manuscript. S. S., C. L. K., A. L. M., and T. M. B. performed experiments and collected data. S. S. and T. R. K. wrote the manuscript. All authors discussed and approved the manuscript.

Acknowledgments—We thank Dr. David R. Emlet and Dr. John A. Kellum (Center for Critical Care Nephrology, University of Pittsburgh) for providing human kidney samples. We also thank Catherine Baty for assistance with imaging studies. The human pon-2 plasmid was a generous gift from Dr. Srinivasa T. Reddy (UCLA, Los Angeles, CA). MEC-4, MEC-10, MEC-2, and MEC-6 cDNAs and the bacterial strain SMC4 were kindly provided by Drs. Monica Driscoll and Laura Bianchi.

References

1. Mackness, M. I., Mackness, B., Durrington, P. N., Connelly, P. W., and Hegele, R. A. (1996) Paraoxonase: biochemistry, genetics and relationship to plasma lipoproteins. *Curr. Opin. Lipidol.* **7,** 69–76
2. Devarajan, A., Shih, D., and Reddy, S. T. (2014) Inflammation, infection, cancer and all that: the role of paraoxonases. *Adv. Exp. Med. Biol.* **824,** 33–41
3. Ng, C. J., Wadleigh, D. J., Gangopadhyay, A., Hama, S., Grijalva, V. R., Navab, M., Fogelman, A. M., and Reddy, S. T. (2001) Paraoxonase-2 is a ubiquitously expressed protein with antioxidant properties and is capable of preventing cell-mediated oxidative modification of low density lipoprotein. *J. Biol. Chem.* **276,** 44444–44449
4. Levy, E., Trudel, K., Bendayan, M., Seidman, E., Delvin, E., Elchebly, M., Lavoie, J. C., Precourt, L. P., Amre, D., and Sinnett, D. (2007) Biological role, protein expression, subcellular localization, and oxidative stress response of paraoxonase 2 in the intestine of humans and rats. *Am. J. Physiol. Gastrointest. Liver Physiol.* **293,** G1252–G1261
5. Devarajan, A., Bourquard, N., Hama, S., Navab, M., Grijalva, V. R., Morvardi, S., Clarke, C. F., Vergnes, L., Reue, K., Teiber, J. F., and Reddy, S. T. (2011) Paraoxonase 2 deficiency alters mitochondrial function and exacerbates the development of atherosclerosis. *Antioxid. Redox Signal.* **14,** 341–351
6. Hagmann, H., Kuczkowski, A., Ruehl, M., Lamkemeyer, T., Brodesser, S., Horke, S., Dryer, S., Schermer, B., Benzing, T., and Brinkkoetter, P. T. (2014) Breaking the chain at the membrane: paraoxonase 2 counteracts lipid peroxidation at the plasma membrane. *FASEB J.* **28,** 1769–1779
7. Horke, S., Witte, I., Wilgenbus, P., Krüger, M., Strand, D., and Förstermann, U. (2007) Paraoxonase-2 reduces oxidative stress in vascular cells and decreases endoplasmic reticulum stress-induced caspase activation. *Circulation* **115,** 2055–2064
8. Horke, S., Witte, I., Wilgenbus, P., Altenhöfer, S., Krüger, M., Li, H., and Förstermann, U. (2008) Protective effect of paraoxonase-2 against endoplasmic reticulum stress-induced apoptosis is lost upon disturbance of calcium homoeostasis. *Biochem. J.* **416,** 395–405
9. Ng, C. J., Bourquard, N., Grijalva, V., Hama, S., Shih, D. M., Navab, M., Fogelman, A. M., Lusis, A. J., Young, S., and Reddy, S. T. (2006) Paraoxonase-2 deficiency aggravates atherosclerosis in mice despite lower apolipoprotein-B-containing lipoproteins: anti-atherogenic role for paraoxonase-2. *J. Biol. Chem.* **281,** 29491–29500
10. Yang, Y., Zhang, Y., Cuevas, S., Villar, V. A., Escano, C., Asico, L. D., Yu, P., Grandy, D. K., Felder, R. A., Armando, I., and Jose, P. A. (2012) Paraoxonase 2 decreases renal reactive oxygen species production, lowers blood pressure, and mediates dopamine D2 receptor-induced inhibition of NADPH oxidase. *Free Radic. Biol. Med.* **53,** 437–446
11. Chelur, D. S., Ernstrom, G. G., Goodman, M. B., Yao, C. A., Chen, L., O'Hagan, R., Chalfie, M. (2002) The mechanosensory protein MEC-6 is a subunit of the *C. elegans* touch-cell degenerin channel. *Nature* **420,** 669–673
12. Harel, M., Aharoni, A., Gaidukov, L., Brumshtein, B., Khersonsky, O., Meged, R., Dvir, H., Ravelli, R. B., McCarthy, A., Toker, L., Silman, I., Sussman, J. L., and Tawfik, D. S. (2004) Structure and evolution of the serum paraoxonase family of detoxifying and anti-atherosclerotic enzymes. *Nat. Struct. Mol. Biol.* **11,** 412–419
13. Gu, G., Caldwell, G. A., and Chalfie, M. (1996) Genetic interactions affecting touch sensitivity in *Caenorhabditis elegans*. *Proc. Natl. Acad. Sci. U.S.A.* **93,** 6577–6582
14. Chalfie, M. (2009) Neurosensory mechanotransduction. *Nat. Rev. Mol. Cell Biol.* **10,** 44–52
15. Driscoll, M., and Chalfie, M. (1991) The mec-4 gene is a member of a family of *Caenorhabditis elegans* genes that can mutate to induce neuronal degeneration. *Nature* **349,** 588–593
16. Huang, M., and Chalfie, M. (1994) Gene interactions affecting mechanosensory transduction in *Caenorhabditis elegans*. *Nature* **367,** 467–470
17. Chen, Y., Bharill, S., Isacoff, E. Y., and Chalfie, M. (2015) Subunit composition of a DEG/ENaC mechanosensory channel of *Caenorhabditis elegans*. *Proc. Natl. Acad. Sci. U.S.A.* **112,** 11690–11695
18. Kellenberger, S., and Schild, L. (2002) Epithelial sodium channel/degenerin family of ion channels: a variety of functions for a shared structure. *Physiol. Rev.* **82,** 735–767
19. Chen, Y., Bharill, S., Altun, Z., O'Hagan, R., Coblitz, B., Isacoff, E. Y., and Chalfie, M. (2016) *Caenorhabditis elegans* paraoxonase-like proteins control the functional expression of DEG/ENaC mechanosensory proteins. *Mol. Biol. Cell* **27,** 1272–1285
20. O'Hagan, R., Chalfie, M., and Goodman, M. B. (2005) The MEC-4 DEG/ENaC channel of *Caenorhabditis elegans* touch receptor neurons transduces mechanical signals. *Nat. Neurosci.* **8,** 43–50
21. Kellenberger, S., and Schild, L. (2015) International Union of Basic and Clinical Pharmacology. XCI. Structure, function, and pharmacology of acid-sensing ion channels and the epithelial Na^+ channel. *Pharmacol. Rev.* **67,** 1–35
22. Warnock, D. G., Kusche-Vihrog, K., Tarjus, A., Sheng, S., Oberleithner, H., Kleyman, T. R., and Jaisser, F. (2014) Blood pressure and amiloride-sensitive sodium channels in vascular and renal cells. *Nat. Rev. Nephrol.* **10,** 146–157

23. Canessa, C. M., Schild, L., Buell, G., Thorens, B., Gautschi, I., Horisberger, J. D., and Rossier, B. C. (1994) Amiloride-sensitive epithelial Na^+ channel is made of three homologous subunits. *Nature* **367,** 463–467
24. Stockand, J. D., Staruschenko, A., Pochynyuk, O., Booth, R. E., and Silverthorn, D. U. (2008) Insight toward epithelial Na+ channel mechanism revealed by the acid-sensing ion channel 1 structure. *IUBMB Life* **60,** 620–628
25. Jasti, J., Furukawa, H., Gonzales, E. B., and Gouaux, E. (2007) Structure of acid-sensing ion channel 1 at 1.9 Å resolution and low pH. *Nature* **449,** 316–323
26. Kashlan, O. B., and Kleyman, T. R. (2011) ENaC structure and function in the wake of a resolved structure of a family member. *Am. J. Physiol. Renal Physiol.* **301,** F684–F696
27. Valentijn, J. A., Fyfe, G. K., and Canessa, C. M. (1998) Biosynthesis and processing of epithelial sodium channels in *Xenopus* oocytes. *J. Biol. Chem.* **273,** 30344–30351
28. Staub, O., Gautschi, I., Ishikawa, T., Breitschopf, K., Ciechanover, A., Schild, L., and Rotin, D. (1997) Regulation of stability and function of the epithelial Na+ channel (ENaC) by ubiquitination. *EMBO J.* **16,** 6325–6336
29. Prince, L. S., and Welsh, M. J. (1998) Cell surface expression and biosynthesis of epithelial Na^+ channels. *Biochem. J.* **336,** 705–710
30. Chanoux, R. A., Robay, A., Shubin, C. B., Kebler, C., Suaud, L., and Rubenstein, R. C. (2012) Hsp70 promotes epithelial sodium channel functional expression by increasing its association with coat complex II and its exit from endoplasmic reticulum. *J. Biol. Chem.* **287,** 19255–19265
31. Grumbach, Y., Bikard, Y., Suaud, L., Chanoux, R. A., and Rubenstein, R. C. (2014) ERp29 regulates epithelial sodium channel functional expression by promoting channel cleavage. *Am. J. Physiol. Cell Physiol.* **307,** C701–C709
32. Kashlan, O. B., Mueller, G. M., Qamar, M. Z., Poland, P. A., Ahner, A., Rubenstein, R. C., Hughey, R. P., Brodsky, J. L., and Kleyman, T. R. (2007) Small heat shock protein αA-crystallin regulates epithelial sodium channel expression. *J. Biol. Chem.* **282,** 28149–28156
33. Buck, T. M., Plavchak, L., Roy, A., Donnelly, B. F., Kashlan, O. B., Kleyman, T. R., Subramanya, A. R., and Brodsky, J. L. (2013) The Lhs1/GRP170 chaperones facilitate the endoplasmic reticulum-associated degradation of the epithelial sodium channel. *J. Biol. Chem.* **288,** 18366–18380
34. Goldfarb, S. B., Kashlan, O. B., Watkins, J. N., Suaud, L., Yan, W., Kleyman, T. R., and Rubenstein, R. C. (2006) Differential effects of Hsc70 and Hsp70 on the intracellular trafficking and functional expression of epithelial sodium channels. *Proc. Natl. Acad. Sci. U.S.A.* **103,** 5817–5822
35. Chanoux, R. A., Shubin, C. B., Robay, A., Suaud, L., and Rubenstein, R. C. (2013) Hsc70 negatively regulates epithelial sodium channel trafficking at multiple sites in epithelial cells. *Am. J. Physiol. Cell Physiol.* **305,** C776–C787
36. Buck, T. M., Kolb, A. R., Boyd, C. R., Kleyman, T. R., and Brodsky, J. L. (2010) The endoplasmic reticulum-associated degradation of the epithelial sodium channel requires a unique complement of molecular chaperones. *Mol. Biol. Cell* **21,** 1047–1058
37. You, H., Ge, Y., Zhang, J., Cao, Y., Xing, J., Su, D., Huang, Y., Li, M., Qu, S., Sun, F., and Liang, X. (2017) Derlin-1 promotes ubiquitination and degradation of epithelial sodium channel (ENaC). *J. Cell Sci.* **130,** 1027–1036
38. Lee, J. W., Chou, C. L., and Knepper, M. A. (2015) Deep sequencing in microdissected renal tubules identifies nephron segment-specific transcriptomes. *J. Am. Soc. Nephrol.* **26,** 2669–2677
39. Fushimi, K., Uchida, S., Hara, Y., Hirata, Y., Marumo, F., and Sasaki, S. (1993) Cloning and expression of apical membrane water channel of rat kidney collecting tubule. *Nature* **361,** 549–552
40. Altenhöfer, S., Witte, I., Teiber, J. F., Wilgenbus, P., Pautz, A., Li, H., Daiber, A., Witan, H., Clement, A. M., Förstermann, U., and Horke, S. (2010) One enzyme, two functions: PON2 prevents mitochondrial superoxide formation and apoptosis independent from its lactonase activity. *J. Biol. Chem.* **285,** 24398–24403
41. Stoltz, D. A., Ozer, E. A., Recker, T. J., Estin, M., Yang, X., Shih, D. M., Lusis, A. J., and Zabner, J. (2009) A common mutation in paraoxonase-2 results in impaired lactonase activity. *J. Biol. Chem.* **284,** 35564–35571
42. Mochizuki, H., Scherer, S. W., Xi, T., Nickle, D. C., Majer, M., Huizenga, J. J., Tsui, L. C., and Prochazka, M. (1998) Human PON2 gene at 7q21.3: cloning, multiple mRNA forms, and missense polymorphisms in the coding sequence. *Gene* **213,** 149–157
43. Bhalla, V., and Hallows, K. R. (2008) Mechanisms of ENaC regulation and clinical implications. *J. Am. Soc. Nephrol.* **19,** 1845–1854
44. Kashlan, O. B., and Kleyman, T. R. (2012) Epithelial Na^+ channel regulation by cytoplasmic and extracellular factors. *Exp. Cell Res.* **318,** 1011–1019
45. Maarouf, A. B., Sheng, N., Chen, J., Winarski, K. L., Okumura, S., Carattino, M. D., Boyd, C. R., Kleyman, T. R., and Sheng, S. (2009) Novel determinants of epithelial sodium channel gating within extracellular thumb domains. *J. Biol. Chem.* **284,** 7756–7765
46. Althaus, M., Bogdan, R., Clauss, W. G., and Fronius, M. (2007) Mechanosensitivity of epithelial sodium channels (ENaCs): laminar shear stress increases ion channel open probability. *FASEB J.* **21,** 2389–2399
47. Morimoto, T., Liu, W., Woda, C., Carattino, M. D., Wei, Y., Hughey, R. P., Apodaca, G., Satlin, L. M., and Kleyman, T. R. (2006) Mechanism underlying flow stimulation of sodium absorption in the mammalian collecting duct. *Am. J. Physiol. Renal Physiol.* **291,** F663–F669
48. Hughey, R. P., Bruns, J. B., Kinlough, C. L., Harkleroad, K. L., Tong, Q., Carattino, M. D., Johnson, J. P., Stockand, J. D., and Kleyman, T. R. (2004) Epithelial sodium channels are activated by furin-dependent proteolysis. *J. Biol. Chem.* **279,** 18111–18114
49. Bruns, J. B., Carattino, M. D., Sheng, S., Maarouf, A. B., Weisz, O. A., Pilewski, J. M., Hughey, R. P., and Kleyman, T. R. (2007) Epithelial Na^+ channels are fully activated by furin- and prostasin-dependent release of an inhibitory peptide from the γ-subunit. *J. Biol. Chem.* **282,** 6153–6160
50. Carattino, M. D., Sheng, S., Bruns, J. B., Pilewski, J. M., Hughey, R. P., and Kleyman, T. R. (2006) The epithelial Na^+ channel is inhibited by a peptide derived from proteolytic processing of its α subunit. *J. Biol. Chem.* **281,** 18901–18907
51. Carattino, M. D., Hughey, R. P., and Kleyman, T. R. (2008) Proteolytic processing of the epithelial sodium channel gamma subunit has a dominant role in channel activation. *J. Biol. Chem.* **283,** 25290–25295
52. Kleyman, T. R., Carattino, M. D., and Hughey, R. P. (2009) ENaC at the cutting edge: regulation of epithelial sodium channels by proteases. *J. Biol. Chem.* **284,** 20447–20451
53. Shi, S., Carattino, M. D., Hughey, R. P., and Kleyman, T. R. (2013) ENaC regulation by proteases and shear stress. *Curr. Mol. Pharmacol.* **6,** 28–34
54. Carattino, M. D., Hill, W. G., and Kleyman, T. R. (2003) Arachidonic acid regulates surface expression of epithelial sodium channels. *J. Biol. Chem.* **278,** 36202–36213
55. Duc, C., Farman, N., Canessa, C. M., Bonvalet, J. P., and Rossier, B. C. (1994) Cell-specific expression of epithelial sodium channel α, β, and γ subunits in aldosterone-responsive epithelia from the rat: localization by *in situ* hybridization and immunocytochemistry. *J. Cell Biol.* **127,** 1907–1921
56. Buck, T. M., Jordahl, A. S., Yates, M. E., Preston, G. M., Cook, E., Kleyman, T. R., and Brodsky, J. L. (2017) Interactions between intersubunit transmembrane domains regulate the chaperone-dependent degradation of an oligomeric membrane protein. *Biochem. J.* **474,** 357–376
57. Grifoni, S. C., McKey, S. E., and Drummond, H. A. (2008) Hsc70 regulates cell surface ASIC2 expression and vascular smooth muscle cell migration. *Am. J. Physiol. Heart Circ. Physiol.* **294,** H2022–H2030
58. Vila-Carriles, W. H., Zhou, Z. H., Bubien, J. K., Fuller, C. M., and Benos, D. J. (2007) Participation of the chaperone Hsc70 in the trafficking and functional expression of ASIC2 in glioma cells. *J. Biol. Chem.* **282,** 34381–34391
59. Johnson, J. L. (2012) Evolution and function of diverse Hsp90 homologs and cochaperone proteins. *Biochim. Biophys. Acta* **1823,** 607–613
60. Cortes-González, C., Barrera-Chimal, J., Ibarra-Sánchez, M., Gilbert, M., Gamba, G., Zentella, A., Flores, M. E., and Bobadilla, N. A. (2010) Opposite effect of Hsp90α and Hsp90β on eNOS ability to produce nitric oxide or superoxide anion in human embryonic kidney cells. *Cell Physiol. Biochem.* **26,** 657–668

61. Mack, K. L., and Shorter, J. (2016) Engineering and evolution of molecular chaperones and protein disaggregases with enhanced activity. *Front. Mol. Biosci.* **3,** 8
62. Ma, H. P., Saxena, S., and Warnock, D. G. (2002) Anionic phospholipids regulate native and expressed epithelial sodium channel (ENaC). *J. Biol. Chem.* **277,** 7641–7644
63. Pochynyuk, O., Staruschenko, A., Tong, Q., Medina, J., and Stockand, J. D. (2005) Identification of a functional phosphatidylinositol 3,4,5-trisphosphate binding site in the epithelial Na^+ channel. *J. Biol. Chem.* **280,** 37565–37571
64. Carattino, M. D., Mueller, G. M., Palmer, L. G., Frindt, G., Rued, A. C., Hughey, R. P., and Kleyman, T. R. (2014) Prostasin interacts with the epithelial Na^+ channel and facilitates cleavage of the γ-subunit by a second protease. *Am. J. Physiol. Renal Physiol.* **307,** F1080–F1087
65. Vuagniaux, G., Vallet, V., Jaeger, N. F., Hummler, E., and Rossier, B. C. (2002) Synergistic activation of ENaC by three membrane-bound channel-activating serine proteases (mCAP1, mCAP2, and mCAP3) and serum- and glucocorticoid-regulated kinase (Sgk1) in *Xenopus* oocytes. *J. Gen. Physiol.* **120,** 191–201
66. Passero, C. J., Mueller, G. M., Myerburg, M. M., Carattino, M. D., Hughey, R. P., and Kleyman, T. R. (2012) TMPRSS4-dependent activation of the epithelial sodium channel requires cleavage of the γ-subunit distal to the furin cleavage site. *Am. J. Physiol. Renal Physiol.* **302,** F1–F8
67. Zhou, H., Chepilko, S., Schütt, W., Choe, H., Palmer, L. G., and Sackin, H. (1996) Mutations in the pore region of ROMK enhance Ba^{2+} block. *Am. J. Physiol.* **271,** C1949–C1956
68. Hoger, J. H., Ilyin, V. I., Forsyth, S., and Hoger, A. (2002) Shear stress regulates the endothelial Kir2.1 ion channel. *Proc. Natl. Acad. Sci. U.S.A.* **99,** 7780–7785
69. Brown, D., Lydon, J., McLaughlin, M., Stuart-Tilley, A., Tyszkowski, R., and Alper, S. (1996) Antigen retrieval in cryostat tissue sections and cultured cells by treatment with sodium dodecyl sulfate (SDS). *Histochem. Cell Biol.* **105,** 261–267